Double-Trap Kinetic Equation for the Oxygen Reduction Reaction on Pt(111) in Acidic Media†

Jia X. Wang,* Junliang Zhang, and Radoslav R. Adzic

Department of Chemistry, Brookhaven National Laboratory, Upton, New York 11973

Received: July 31, 2007; In Final Form: September 18, 2007

We derived an intrinsic kinetic equation for the four-electron oxygen reduction reaction (ORR) in acidic media using free energies of activation and adsorption as the kinetic parameters. Our kinetic model consists of four essential elementary reactions: a dissociative adsorption (DA) and a reductive adsorption (RA), which yield two reaction intermediates, O and OH; a reductive transition (RT) from O to OH; and a reductive desorption (RD) of OH. Analytic expressions were found for the O and OH adsorption isotherms by solving the steady-state rate equations. For the ORR on Pt(111) in 0.1 M $HClO_4$ solution, we analyzed the measured polarization curves, thereby deducing activation free energies that are consistent with the values from theoretical calculations. The reductive adsorption (ΔG_{RA}^{*0}= 0.46 eV) is not the rate-determining step (RDS) for the ORR on Pt because dissociative adsorption (ΔG_{DA}^{*0}= 0.26 eV) offers a more favorable pathway at high potentials. It, however, generates strongly adsorbed O. The high activation barriers for the O to OH transition (ΔG_{RT}^{*0}= 0.50 eV) and OH desorption (ΔG_{RD}^{*0}= 0.45 eV) cause a large potential loss for the desorption-limited ORR. As the OH coverage increases to a constant value with decreasing potential, the Tafel slope increases to the value determined by a symmetric electron-transfer coefficient. We discuss the role of adsorption isotherm in kinetic analysis and, via activity-and-barrier plots, illustrate why the RDS may vary with reaction conditions or may not exist. Recognizing such features of electrocatalytic reactions can facilitate reaching the long-standing goal of quantitative descriptions and predictions of electrocatalysts' activities.

1. Introduction

The four-electron (4e) oxygen reduction reaction (ORR) in acidic media has been investigated for decades partly because of its importance in energy technology as the cathodic reaction in proton-exchange membrane fuel cells.[1−8] Recent efforts focused on developing active, stable, and inexpensive ORR electrocatalysts.[9−13] However, realizing this combination of requirements greatly challenges researchers, necessitating a deeper understanding of the reaction mechanisms and factors governing catalytic behavior.

Advances in computer technology and in algorithms for calculating electron structure have delivered detailed energetic information about the elementary reactions in the ORR, Shi et al.'s recently discussed.[14] For example, the adsorption free energies were assessed for several reaction intermediates using density functional theory (DFT) calculations to illustrate possible reaction pathways and rate-determining steps (RDS).[15] Moreover, the relationship between activation energies and adsorption energies was examined,[16] and the former were expressed as a function of potential for the ORR's four elementary reactions.[17] In addition, *ab initio* molecular-dynamics simulations illustrated the role of proton transfer in the ORR kinetics.[18] So far, theoretical predictions of the catalysts' activities were based upon single RDS approximation.[15,19] By developing intrinsic kinetic equations using adsorption and activation free energies as the kinetic parameters, we can directly connect theory and experiment.

Semiempirical kinetic equations for the ORR were proposed by assuming that the first 1e-reduction in the adsorption process was the RDS.[1,7,20,21] Combined with the experimentally deduced adsorption isotherm for OH and bisulfate, we fitted the measured polarization curves for Pt(111) in $HClO_4$ and H_2SO_4 solutions.[22] Our findings support the idea that the adsorption of OH and O causes the Tafel slope to deviate from 118 mV/decade at room temperature. However, these semiempirical approaches cannot convincingly explain why the Tafel slope commonly is considered to be only half of that value in fuel cell modeling.

In this study, we derived a double-trap kinetic equation for the 4e-ORR in acidic media using the methodology we developed in obtaining the dual-pathway kinetic equation for the hydrogen oxidation reaction (HOR).[23,24] Our approach differs from previous kinetic modeling in that we carefully chose the essential elementary reactions without assuming one as the RDS because assuming a single RDS may not hold over a wide potential region for reactions that either have more than one pathway or have several comparable activation barriers. These situations are important because catalytic activities are improved by finding new ways to bypass the major activation barrier and manipulating the electronic structure of a catalyst to lower the highest activation barrier. While the HOR case exemplified an RDS varying with potential due to the dual pathways for adsorption, the ORR on Pt(111) discussed here represents a situation wherein the strong adsorption of O and OH acts as a

† Part of the "Giacinto Scoles Festschrift".

* To whom correspondence should be addressed. E-mail: jia@bnl.gov. Tel: +1-631-344-2515. Fax: +1-631-344-5815.

10.1021/jp076104e CCC: $37.00
Published on Web 12/06/2007

double-trap, generating two major barriers for the desorption-limited ORR.

2. Kinetic Model and Equations for the 4e-ORR in Acidic Media

For the 4e-ORR, $O_2 + 4H^+ + 4e^- \rightleftarrows 2H_2O$, we proposed four essential elementary reactions:

$$^1/_2O_2 \rightleftarrows O_{ad} \quad \text{dissociative adsorption (DA)} \tag{1}$$

$$^1/_2O_2 + H^+ + e^- \rightleftarrows OH_{ad} \quad \text{reductive adsorption (RA)} \tag{2}$$

$$O_{ad} + H^+ + e^- \rightleftarrows OH_{ad} \quad \text{reductive transition (RT)} \tag{3}$$

$$OH_{ad} + H^+ + e^- \rightleftarrows H_2O \quad \text{reductive desorption (RD)} \tag{4}$$

These represent two adsorption pathways: one is through dissociative adsorption (DA) that forms adsorbed O, followed by a reductive transition (RT) from O to OH; the other is through reductive adsorption (RA) in which first electron transfer coincides with adsorption. In both cases, the electrocatalytic reaction is completed by the reductive desorption (RD) of OH. Schematically, they can be shown as

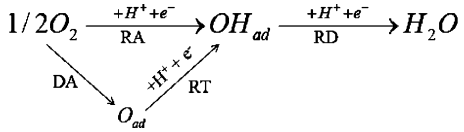

We ignore other possible reaction intermediates, such as physisorbed O_2 and associated O_2H, because they are much less stable than O and OH. Our IR study revealed O_2^- on Pt in alkaline solution, but no O_2H in acidic solution.[25] The fractional stoichiometric number is used in eqs 1 and 2 to simplify the expression for reactions $O_2 \rightleftarrows 2O_{ad}$ and $O_2 + H^+ + e^- \rightleftarrows OH_{ad} + O_{ad}$, so eliminating the quadratic terms for θ_O and θ_{OH} in the rate equations (see the List of Symbols):

$$\nu_{DA} = k_{DA}c_{O_2}^{1/2}(1 - \theta_O - \theta_{OH}) - k_{-DA}\theta_O \tag{5}$$

$$\nu_{RA} = k_{RA}c_{O_2}^{1/2}c_{H^+}e^{-E/2kT}(1 - \theta_O - \theta_{OH}) - k_{-RA}e^{E/2kT}\theta_{OH} \tag{6}$$

$$\nu_{RT} = k_{RT}c_{H^+}e^{-E/2kT}\theta_O - k_{-RT}e^{E/2kT}\theta_{OH} \tag{7}$$

$$\nu_{RD} = k_{RD}c_{H^+}e^{-E/2kT}\theta_{OH} - k_{-RD}e^{E/2kT}(1 - \theta_O - \theta_{OH}) \tag{8}$$

Although employing the fractional stoichiometric number does not change the concentration dependence of the reversible potential, it entails a different reaction order in the kinetic equations. For the HOR, we examined kinetic models with the dissociative adsorption of hydrogen written as $H_2 \rightleftarrows 2H_{ad}$ or $^1/_2H_2 \rightleftarrows H_{ad}$ corresponding to a quadratic or linear term on θ_H. The latter failed to fit the experimental data because the DA reaction is the RDS for the HOR at small overpotentials where the fast rise of kinetic current requires a quadratic dependence on θ_H. For the ORR, we found that the O to OH transition and OH desorption play more important roles in determining the kinetic behavior than do the DA and RA reactions; thus, the reaction order in these two adsorption reactions is undeterminable from analyzing polarization curves. We chose to use the linear expression for simplicity, considering it to be a justifiable approximation to the true reaction mechanism supported by theory or other experimental evidence.

The total kinetic current, j_k, is proportional to the sum of the reaction rates for those involving 1e-reduction. By combining this formula with the steady-state rate equations,

$$d\theta_O/dt = \nu_{DA} - \nu_{RT} = 0 \tag{9}$$

$$d\theta_{OH}/dt = \nu_{RA} + \nu_{RT} - \nu_{RD} = 0 \tag{10}$$

we obtain

$$\begin{aligned} j_k &= F(\nu_{RA} + \nu_{RT} + \nu_{RD}) \\ &= 2F\nu_{RD} = 2F(\nu_{RA} + \nu_{RT}) = 2F(\nu_{DA} + \upsilon_{RA}) \\ &= j_{RD} = j_{RA} + j_{RT} = j_{DA} + j_{RA} \end{aligned} \tag{11}$$

where F is the Faraday constant and $j_i = 2F\nu_i$ is the kinetic current for a single elementary reaction. At the reversible potential for the ORR or zero overpotential, $\eta = E - E^0 = 0$, the net current is zero, which leads to $\nu_{RD} = \nu_{+RD} - \nu_{-RD} = 0$ and $\nu_{DA} = \nu_{RT} = -\nu_{RA}$. Although not immediately obvious, the net reaction rate also is zero for the DA, RT, and RA reactions at $\eta = 0$, as shown in the Appendix.

Applying the methodology we developed in deriving the HOR kinetic equation,[24] we define the intrinsic exchange currents and correlate them with the activation free energies:

$$j_{DA}^0 = 2Fk_{DA}c_{O_2}^{1/2} = j^*e^{-\Delta G_{DA}^{*0}/kT} \tag{12}$$

$$j_{RA}^0 = 2Fk_{RA}c_{O_2}^{1/2}c_{H^+} = j^*e^{-\Delta G_{RA}^{*0}/kT} \tag{13}$$

$$j_{RT}^0 = 2Fk_{RT}c_{H^+} = j^*e^{-\Delta G_{RT}^{*0}/kT} \tag{14}$$

$$j_{RD}^0 = 2Fk_{RD}c_{H^+} = j^*e^{-\Delta G_{RD}^{*0}/kT} \tag{15}$$

Here, the superscript "0" represents the zero overpotential and $j^* = 1000$ A cm^{-2} is the chosen reference prefactor setting the scale for activation free energy, just as the reference electrode sets the scale for the potential.[24]

Replacing the rate constants and concentrations in the solution phase with activation free energies at zero overpotential allows us to express the rate of a reaction by the product of its intrinsic rate and the coverage of its reactant. Hence, we rewrite eqs 5−8 as

$$j_{DA} = j^*e^{-\Delta G_{DA}^*/kT}(1 - \theta_O - \theta_{OH}) - j^*e^{-\Delta G_{-DA}^*/kT}\theta_O \tag{16}$$

$$j_{RA} = j^*e^{-\Delta G_{RA}^*/kT}(1 - \theta_O - \theta_{OH}) - j^*e^{-\Delta G_{-RA}^*/kT}\theta_{OH} \tag{17}$$

$$j_{RT} = j^*e^{-\Delta G_{RT}^*/kT}\theta_O - j^*e^{-\Delta G_{-RT}^*/kT}\theta_{OH} \tag{18}$$

$$j_{RD} = j^*e^{-\Delta G_{RD}^*/kT}\theta_{OH} - j^*e^{-\Delta G_{-RD}^*/kT}(1 - \theta_O - \theta_{OH}) \tag{19}$$

The intrinsic rates, $g_i \equiv e^{-\Delta G_i^*/kT}$ (the minus sign in the subscript represents the backward reaction), are determined solely by their activation barriers. In other words, it is the rate of a reaction when the surface is fully covered by its reactant, e.g., O for the RT, OH for the RD, and empty surface sites for the RA and DA reactions in the forward direction. Not all eight activation free energies are independent because the one for a backward reaction can be linked with its for ward reaction by the adsorption free energies for the reaction intermediates at $\eta = 0$, which are determined by the equilibrium

coverage for the O and OH,

$$\frac{\theta_O^0}{1-\theta_O^0-\theta_{OH}^0} = e^{-\Delta G_O^0/kT} \tag{20}$$

$$\frac{\theta_{OH}^0}{1-\theta_O^0-\theta_{OH}^0} = e^{-\Delta G_{OH}^0/kT} \tag{21}$$

Therefore, the potential-dependent activation free energies can be expressed as

$$\Delta G_{DA}^* = \Delta G_{DA}^{*0} \tag{22}$$

$$\Delta G_{RA}^* = \Delta G_{RA}^{*0} - \beta e(E^0 - E) \tag{23}$$

$$\Delta G_{RT}^* = \Delta G_{RT}^{*0} - \beta e(E^0 - E) \tag{24}$$

$$\Delta G_{RD}^* = \Delta G_{RD}^{*0} - \beta e(E^0 - E) \tag{25}$$

$$\Delta G_{-DA}^* = \Delta G_{DA}^{*0} - \Delta G_O^0 \tag{26}$$

$$\Delta G_{-RA}^* = \Delta G_{RA}^{*0} - \Delta G_{OH}^0 + (1-\beta)e(E^0 - E) \tag{27}$$

$$\Delta G_{-RT}^* = \Delta G_{RT}^{*0} - \Delta G_{OH}^0 + \Delta G_O^0 + (1-\beta)e(E^0 - E) \tag{28}$$

$$\Delta G_{-RD}^* = \Delta G_{RD}^{*0} + \Delta G_{OH}^0 + (1-\beta)e(E^0 - E) \tag{29}$$

The free energy diagram at $\eta = 0$ shown in Figure 1d illustrates how the activation free energies for the backward reactions (the length of dashed vertical lines) are determined by the four activation free energies (ΔG_{DA}^{*0}, ΔG_{RA}^{*0}, ΔG_{RT}^{*0}, and ΔG_{RD}^{*0}) for the forward directions (the length of solid vertical lines) and two adsorption free energies for the intermediates (ΔG_O^0 and ΔG_{OH}^0).

The total kinetic current can be expressed using $j_k = j_{RD}$ (eqs 11, 19, 25, and 29),

$$j_k = j^* e^{-\Delta G_{RD}^{*0}/kT} e^{\beta(E^0-E)/kT}\theta_{OH} - j^* e^{-(\Delta G_{RD}^{*0}+G_{OH}^0)/kT} e^{-(1-\beta)(E^0-E)/kT}(1-\theta_O-\theta_{OH}) \tag{30}$$

When the backward reaction rate is negligible and assuming $\beta = 0.5$, the kinetic equation can be simplified to

$$j_k \cong j_f = j^* e^{-\Delta G_{RD}^{*0}/kT} e^{(E^0-E)/2kT}\theta_{OH} \tag{31}$$

Under this condition,

$$j = \frac{j_k}{1+j_f/j_L} \cong \frac{j_k}{1+j_k/j_L} \quad \text{and thus } j_k = \frac{j}{1-j/j_L} \tag{32}$$

where j and j_L are the measured and mass-transport-limited currents, respectively.[23] That is, the ORR kinetic current can be obtained by fitting the measured polarization curves or by numerically converting the data using eq 32. Alternatively, the kinetic current can be expressed as the sum of the currents of two adsorption pathways (backward reactions omitted),

$$j_k = j_{DA} + j_{RA} \cong j^* e^{-\Delta G_{DA}^{*0}/kT}(1-\theta_O-\theta_{OH}) + j^* e^{-\Delta G_{RA}^{*0}/kT} e^{(E^0-E)/2kT}(1-\theta_O-\theta_{OH}) \tag{33}$$

Next, we derive the adsorption isotherms, $\theta_O(E)$ and $\theta_{OH}(E)$, from the steady-state rate equations. Combining eqs 16−19 with eqs 9−10 leads to (note that $j_i = 2F\nu_i$ and $g_i = e^{-\Delta G_i^*/kT}$)

$$g_{DA}(1-\theta_O-\theta_{OH}) - g_{-DA}\theta_O - g_{RT}\theta_O + g_{-RT}\theta_{OH} = 0 \tag{34}$$

$$g_{RA}(1-\theta_O-\theta_{OH}) - g_{-RA}\theta_{OH} + g_{RT}\theta_O - g_{-RT}\theta_{OH} - g_{RD}\theta_{OH} + g_{-RD}(1-\theta_O-\theta_{OH}) = 0 \tag{35}$$

which can be rearranged into a pair of linear equations

$$(g_{DA}+g_{-DA}+g_{RT})\theta_O + (g_{DA}-g_{-RT})\theta_{OH} - g_{DA} \equiv a_1\theta_O + b_1\theta_{OH} - c_1 = 0 \tag{36}$$

$$(g_{RA}-g_{RT}+g_{-RD})\theta_O + (g_{RA}+g_{-RA}+g_{-RT}+g_{RD}+g_{-RD})\theta_{OH} - (g_{RA}+g_{-RD}) \equiv a_2\theta_O + b_2\theta_{OH} - c_2 = 0 \tag{37}$$

whose solutions give the analytical expressions for the O and OH adsorption isotherms:

$$\theta_O = \frac{c_1b_2 - c_2b_1}{a_1b_2 - a_2b_1} \tag{38}$$

$$\theta_{OH} = \frac{c_1a_2 - c_2a_1}{b_1a_2 - b_2a_1} \tag{39}$$

For $\eta \to \infty$, or at sufficiently low potentials, g_{RA}, g_{RT}, $g_{RD} \gg g_{DA}$, $g_{-DA} \gg g_{-RA}$, g_{-RT}, g_{-RD}. Thus,

$$\theta_O^\infty \to \frac{g_{DA}g_{RD}}{g_{RT}(g_{RA}+g_{RD}+g_{DA})} = 0 \tag{40}$$

$$\theta_{OH}^\infty \to \frac{1}{1+g_{RD}/g_{RA}} = \frac{1}{1+e^{(\Delta G_{RA}^{*0}-\Delta G_{RD}^{*0})/kT}} \tag{41}$$

At $\eta = 0$, we find the equilibrium coverage (from eqs 20 and 21),

$$\theta_O^0 = \frac{e^{-\Delta G_O^0/kT}}{1+e^{-\Delta G_O^0/kT}+e^{-\Delta G_{OH}^0/kT}} \tag{42}$$

$$\theta_{OH}^0 = \frac{e^{-\Delta G_{OH}^0/kT}}{1+e^{-\Delta G_O^0/kT}+e^{-\Delta G_{OH}^0/kT}} \tag{43}$$

and thus, the exchange current

$$j_0 = j_{RD}^0\,\theta_{OH}^0 = \frac{j^* e^{-\Delta G_{RD}^{*0}/kT}}{e^{\Delta G_{OH}^0} + e^{(\Delta G_{OH}^0 - \Delta G_O^0)/kT} + 1} \tag{44}$$

Below, we first present the results of a kinetic analysis using the double-trap kinetic model described above, with the sym-

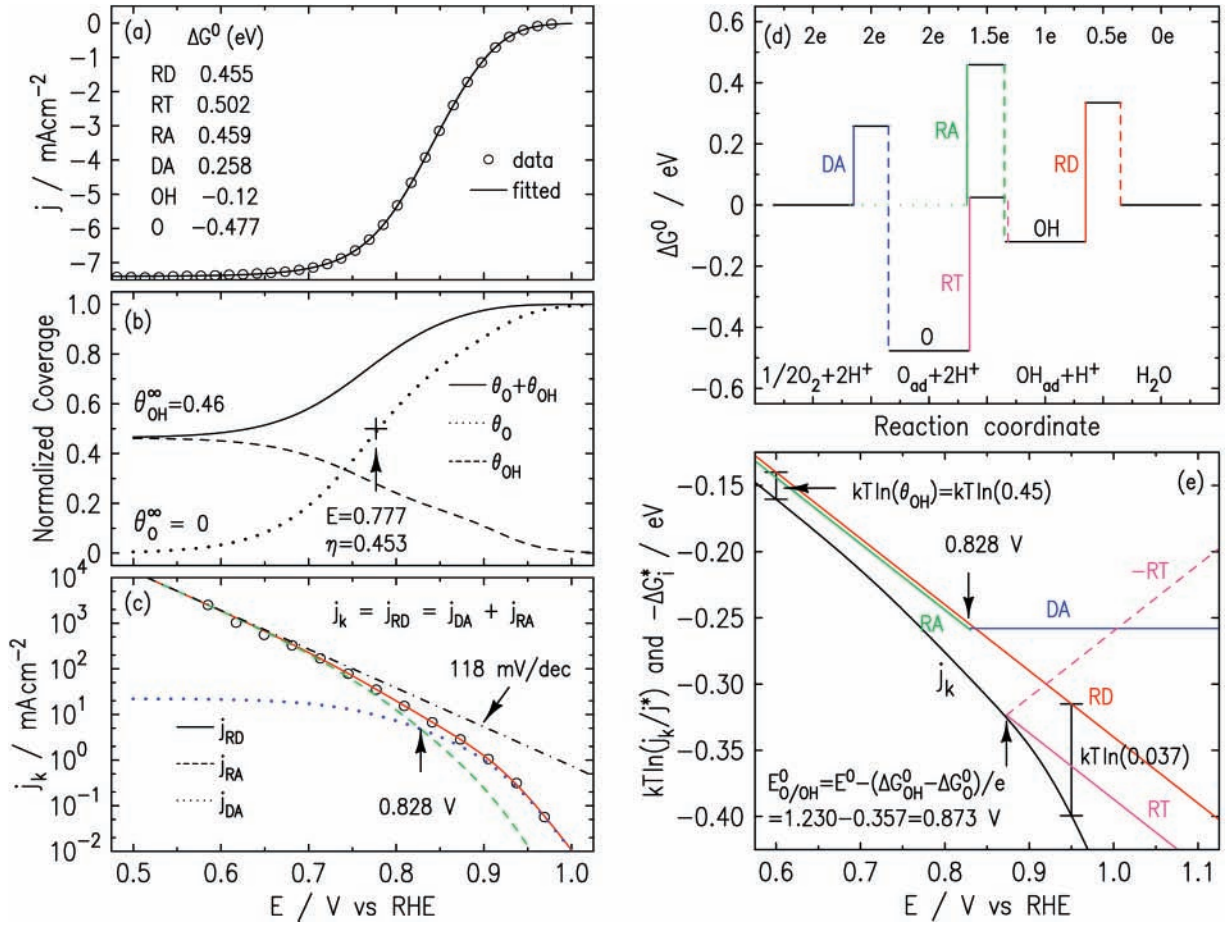

Figure 1. (a) ORR polarization curve measured at 296 K using a Pt(111) rotating disk electrode (2500 rpm) in oxygen-saturated (1 atm) 0.1 M $HClO_4$ solution. The parameters of the best fit given in (a) were used to calculate the adsorption isotherms for O, OH, and their sum in (b), and, the kinetic currents in (c). (d) Free energy diagram at $\eta = 0$ constructed using the fitted activation free energies for the forward reactions (represented by the lengths of the solid vertical lines) and the adsorption free energies for O and OH (the values on the *y*-axis for the horizontal bars). The lengths of dashed vertical lines represent the activation free energies of the backward reactions. (e) Activity-and-barrier plot showing the kinetic current (black line) and the activation free energies (colored lines) on an equivalent energy scale. Note, the higher that a $-\Delta G^*$ curve rises, the lower is the activation barrier, and thus, the higher is the reaction rate or the kinetic current.

metric electron-transfer coefficient, i.e., $\beta = 0.5$, in the next section. In section 4, we discuss the adsorption isotherm and the elimination of the models with single pathway and with asymmetric coefficients.

3. Activation Free Energies for the ORR on Pt(111)

Figure 1a shows an ORR polarization curve for Pt(111) measured in an oxygen-saturated 0.1 M $HClO_4$ solution. Excellent fits are obtained with ΔG^0_{OH} and ΔG^{*0}_{RD} fixed at certain values, while allowing ΔG^0_O, ΔG^{*0}_{DA}, ΔG^{*0}_{RA}, and ΔG^{*0}_{RT} to vary. For $\Delta G^0_{OH} = -0.12$ eV, ΔG^{*0}_{RD} can be between 0.445 and 0.465 eV, whereas for $\Delta G^{*0}_{RD} = 0.455$ eV, ΔG^0_{OH} can range from -0.13 to $+0.10$ eV. As the first three rows of Table 1 show, the uncertainty in ΔG^{*0}_{RD}, ± 0.01 eV, generates a similar uncertainty in the other four fitted free energies. The OH coverage at infinite overpotential, θ^∞_{OH}, varies from 0.69 to 0.31 with decreasing ΔG^{*0}_{RD}. In contrast, the value of ΔG^0_{OH} affects only the value of ΔG^0_O (the last two rows in Table 1). The lack of experimental methods to determine the equilibrium coverage, θ^0_O, and θ^0_{OH} under the ORR conditions, is responsible for the large uncertainty in the adsorption free energies on an absolute scale. We chose $\Delta G^0_{OH} = -0.12$ eV to be sure that the total coverage of O and OH reaches unity at zero overpotential irrespective of the value for ΔG^0_O (see eqs 42 and 43).

TABLE 1: Several Sets of Free Energies Producing Excellent Fits to the ORR Polarization Curve in Figure 1a[a]

ΔG^{*0}_{RD}	ΔG^0_{OH}	ΔG^0_O	ΔG^{*0}_{DA}	ΔG^{*0}_{RA}	G^{*0}_{RT}	θ^∞_{OH}
0.465	*−0.12*	−0.467	0.244	0.445	0.500	0.69
0.455	**−0.12**	**−0.477**	**0.258**	**0.459**	**0.502**	**0.46**
0.445	*−0.12*	−0.487	0.264	0.465	0.504	0.31
0.455	*−0.13*	−0.487	0.258	0.459	0.502	0.46
0.455	*0.10*	−0.257	0.258	0.459	0.502	0.46

[a] The values for ΔG^0_{OH} and ΔG^{*0}_{RD} in the first two columns (italics) were fixed; the other four were adjusted during fitting. The values in bold are used in Figure 1.

Table 2 lists the free energies determined by fitting the polarization curves measured with electrode rotating rates of 1600 and 2500 rpm at potential sweep rates of 50 and 20 mV/s. The differences are significant when measurements for different catalysts are compared but do not change the major conclusions of this study. Lowering the potential sweep rate caused a small decline in the deduced kinetic currents that could be attributed to an increase of O coverage with time.

Figure 1b shows the adsorption isotherms, θ_{OH}, θ_O, and $\theta^0_O + \theta^0_{OH}$, calculated using the parameters from Figure 1a. Interestingly, the overpotential for $\theta_O = 0.5$ is 0.453 V, close to the value of 0.455 eV for ΔG^{*0}_{RD}. This is similar to the finding for the HOR where the overpotential for $\theta_H/\theta^0_H = 0.5$ is near the activation free energy for H desorption.[24] The rise

TABLE 2: Free Energies Determined from Fitting the Polarization Curves Measured at Different Electrode Rotating Rates and Potential Sweep Rates with ΔG^0_{OH} and ΔG^{*0}_{RD} Fixed at −0.12 and 0.455 eV, Respectively[a]

ω, rpm	dE/dt, mV/s	ΔG^0_O, eV	ΔG^{*0}_{DA}, eV	ΔG^{*0}_{RA}, eV	ΔG^{*0}_{RT}, eV	$j_{k(0.8V)}$, mA cm^{-2}	$j_{k(0.85V)}$, mA cm^{-2}	$j_{k(0.9V)}$, mA cm^{-2}
1600	50	−0.476	0.268	0.458	0.506	21.0	5.45	1.25
2500	50	−0.477	0.258	0.459	0.502	19.6	5.41	1.27
1600	20	−0.482	0.232	0.427	0.514	15.4	4.28	1.00
2500	20	−0.483	0.251	0.450	0.514	16.9	3.95	1.01

[a] The corresponding kinetic currents are given for three different potentials.

of θ^0_{OH} with *decreasing* potential to a constant value seems counterintuitive because anion adsorption in general decreases with decreasing potential. However, when O is adsorbed more strongly than OH at high potentials, it desorbs with decreasing potential, which opens more surface sites and can then result in an increase of OH coverage. At sufficiently low potentials, the OH coverage approaches a value determined by eq 41. That is, $\theta^\infty_{OH} = 0.5$ when $\Delta G^{*0}_{RA} = \Delta G^{*0}_{RD}$, and $\theta^\infty_{OH} > 0.5$ when $\Delta G^{*0}_{RA} < \Delta G^{*0}_{RD}$. Thus, the greater the barrier for the RD reaction as compared to that for the RA reaction, the more OH will occupy surface sites, equalizing the reaction rates for the two steps because the OH acts both as a site-blocker for the RA reaction and as the reactant for the RD reaction.

Figure 1c shows the $\log(j_k)-E$ plot. The close agreement between the data converted via eq 32 (circles) and the calculated kinetic current (solid line) indicates that the backward reaction rate is negligibly low so that $j_k = j_f$ holds true for the ORR on Pt. The plot also reveals that the Tafel slope increases continuously with decreasing potential to the nominal value for $\beta = 0.5$ as θ_{OH} approaches a constant value.

To elucidate the relationships among the six free energies and their roles in determining the kinetic current, we display the free energy diagram at zero overpotential in Figure 1d and their potential dependence in Figure 1e. In the former, the lengths of the colored vertical lines represent the values of the activation free energies, and the *y*-axis values of the horizontal bars show the adsorption free energies for O and OH. Thus, the highest activation free energy is that of the RT reaction (0.502 eV, purple), followed quite closely by the 0.46 eV and the 0.45 eV activation energies of the RA (green) and RD (red) reactions, respectively. Similarly, the lengths of the dashed lines show the activation free energies of the backward reactions that are determined by the two adsorption free energies and four activation free energies of the forward reactions.

Because the change of activation free energies is the driving force for an increasing kinetic current with decreasing potential, it is useful to make them directly comparable. Figure 1e plots, on the same scale, the activity in terms of $kT\ln(j_k/j^*)$ and the activation free energies in negative value, $-\Delta G^*$. Here, the activity curve goes up with the rise of the $-\Delta G^*$ curves because they represent the fall of activation barriers. This activity-and-barrier plot quantitatively describes the reaction mechanism.

Among the four solid colored lines for the forward reactions, three rise with decreasing potential and one remains constant because the RA, RT, and RD reactions involve a reductive electron transfer, but the DA reaction does not. The DA line at high potentials and the RA line at low potentials show the smaller of the two barriers for adsorption. The potential where they are equal (0.828 V) corresponds to the crossing potential for j_{DA} and j_{RA} in Figure 1c. The fact that the RD and RT lines are lower than the DA line at high potentials indicates that the ORR activity on Pt is desorption-limited. The RT line is shown at potentials above where it intercepts the −RT line. This potential denotes the reversible potential for the O and OH

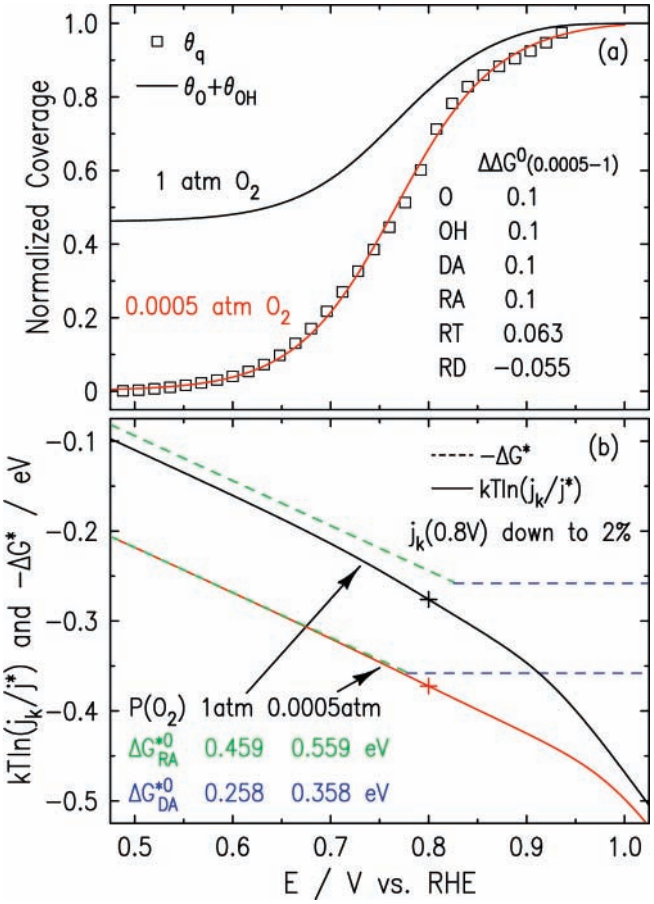

Figure 2. (a) Coverage of oxygen-containing species deduced from integrated charge, θ_q, measured for Pt(111) at 50 mV/s in deaerated 0.1 M $HClO_4$ solution, and the fit (red line) using $\theta_O + \theta_{OH}$ with ΔG^0_O, ΔG^0_{OH}, ΔG^{*0}_{DA}, and ΔG^{*0}_{RA} fixed while allowing ΔG^{*0}_{RT} and ΔG^{*0}_{RD} to vary. (b) Activity-and-barrier plot showing that the expected changes in the activation barriers (dashed lines) due to a decrease in oxygen concentration cause a drop of kinetic current (solid lines).

transition; that is, when $\Delta G^*_{RT} = \Delta G^*_{-RT}$ we find, from eqs 24 and 28,

$$E^{rev}_{O/OH} = E^0 - (\Delta G^0_{OH} - \Delta G^0_O)/e \tag{45}$$

where $E^0 = 1.230$ V at 296 K, and hence, $E^{rev}_{O/OH} = 1.230 - 0.357 = 0.873$ V. Above this potential, the RT reaction is favorable in the backward direction causing a high O coverage, and thus, a low kinetic current. From eqs 31 and 25, we find

$$kT\ln(j_k/j^*) = -\Delta G^*_{RD} + kT\ln(\theta_{OH}) \tag{46}$$

That is, the gap between the $kT\ln(j_k/j^*)$ and the $-\Delta G^*_{RD}$ curves is $kT\ln(\theta_{OH})$. Because θ_{OH} approaches 0.46 at sufficiently low potentials, the minimum gap is $kT\ln(0.46) = -0.02$ eV. At high potentials, the gap increases with decreasing θ_{OH}, which then causes the Tafel slope to decline.

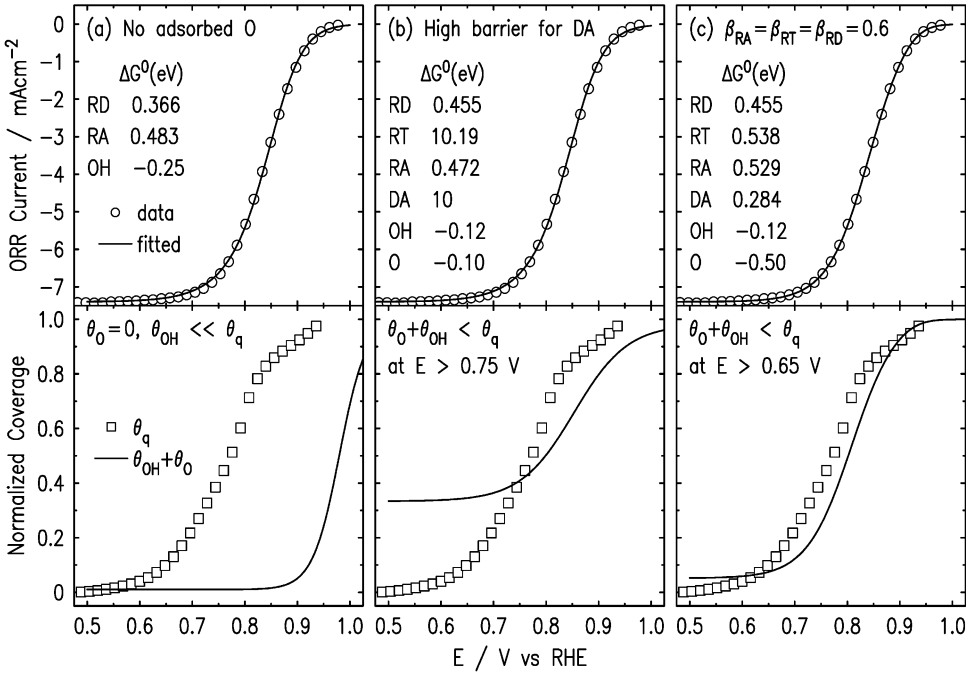

Figure 3. Fits to the measured polarization curve for the ORR on Pt(111) using three different models (upper panel), and their corresponding adsorption isotherms compared to θ_q (lower panel).

Our discussion shows that reductive adsorption is not the RDS for the ORR on Pt because dissociative adsorption affords the more active pathway at high potentials. The resulting reaction intermediates, O and OH, are strongly bonded on the Pt surface, requiring considerable overpotential to overcome the barriers for the O to OH transition and OH desorption. Thus, the ORR is desorption-limited. This conclusion is consistent with the fact that ORR activities are enhanced when O and OH adsorption weakens. Next, we compare the calculated and experimentally deduced activation barriers.

Nørskov et al.'s DFT-calculated values for ΔG_1 and ΔG_2, viz., 0.45 and 0.43 3V at pH 0, are equivalent to the minimum values for our ΔG_{RT}^{*0} and ΔG_{RD}^{*0}, respectively.[15] According to $\Delta(\Delta G) = kT \ln(10) \times \text{pH} = 0.06$ pH for proton-transfer reactions, the values for pH = 1 are 0.51 and 0.49 eV, respectively, close to the corresponding values $\Delta G_{RT}^{*0} = 0.502$ eV and $\Delta G_{RD}^{*0} = 0.455$ eV determined from our analysis of the polarization curve measured in 0.1 M $HClO_4$.

There is considerable uncertainty about the activation free energy for the DA reaction because it strongly depends on the coverage of O and OH. Nørskov and colleagues calculated the activation barrier using $E_a^{diss} = 1.8\Delta E_O - 2.89$, where ΔE_O is the binding energy of O on Pt.[15] Because ΔE_O equals 1.57 and 2.36 eV, respectively, for a 0.25 and 0.5 atomic monolayer, E_a^{diss} varies from −0.06 to +1.36 eV depending on the coverage. Our value of 0.258 eV lies within the range of these theoretical calculations. Protonation is involved in the RA reaction in addition to the O−O bond break as in the DA reaction, and so these authors estimated a 0.13 eV higher activation free energy for the former at pH = 0. Our measurements were carried out at pH = 1; hence, the difference would be 0.13 + 0.06pH = 0.19 eV. This predicted value is close to our result, $\Delta G_{RA}^{*0} - \Delta G_{DA}^{*0} = 0.459 - 0.258 = 0.201$ eV. Other theoretical studies reported different activation energies for the RA reaction, which are not very different from our value of 0.459 eV, ranging from 0.22 eV (Hyman and Medlin)[26] to 0.4 eV (Wang and Balbuena)[18] and 0.45 eV (Anderson et al.).[27]

Wakabayashi et al. measured the temperature-dependence of ORR activity at a Pt film electrode, obtaining 38 kJ/mol for the apparent activation energy at −0.525 V versus E^0.[28] For T = 296 K, 38 kJ/mol equals 0.394 eV, which is very close to our estimate of 0.386 eV. In calculating this value, we assumed that at 1.23 − 0.525 = 0.705 V, the highest activation free energy in the dominant pathway is $\Delta G_{RA}^{*0} - \eta/2 = 0.458 - 0.525/2 = 0.196$ eV for the RA reaction, and that $T\Delta S = 0.19$ eV for pH = 1; thus, $\Delta H = \Delta G + T\Delta S = 0.196 + 0.19 = 0.386$ eV.

4. Kinetics-Deduced Adsorption Isotherm

Further support for the dual-path model with a symmetric electron-transfer coefficient lies in the agreement between the kinetics-deduced and the measured adsorption isotherm for the ORR intermediates. For the HOR, we showed that the H coverage should, and can, be measured under the HOR condition.[24] However, there is so far no O- and OH-specific method for *in situ* monitoring. Even the total charge for O and OH adsorption can only be measured in the absence of oxygen because the ORR current is not the same and thus cannot be subtracted out from polarization measurements at different potential sweep rates. Thus, we used the adsorption isotherm deduced from integrated charge obtained in deaerated solution in analysis.

Figure 2a shows the normalized coverage deduced from the integrated charge, θ_q, measured for Pt(111) at 50 mV/s in deaerated 0.1 M $HClO_4$ solution. Assuming 1e per adsorbate, the maximum coverage measured is slightly lower than a 0.5 atomic monolayer.[22] The black lines show the calculated adsorption isotherm using the parameters determined from fitting the measured polarization curve. The curve for the total coverage, $\theta_O + \theta_{OH}$, is higher than θ_q at all potentials, which is expected because $\theta_O + \theta_{OH}$ should increase with O_2 concentration. The activation free energies for the adsorption reactions and the adsorption free energies for O and OH increase as the oxygen concentration falls. Assuming that oxygen

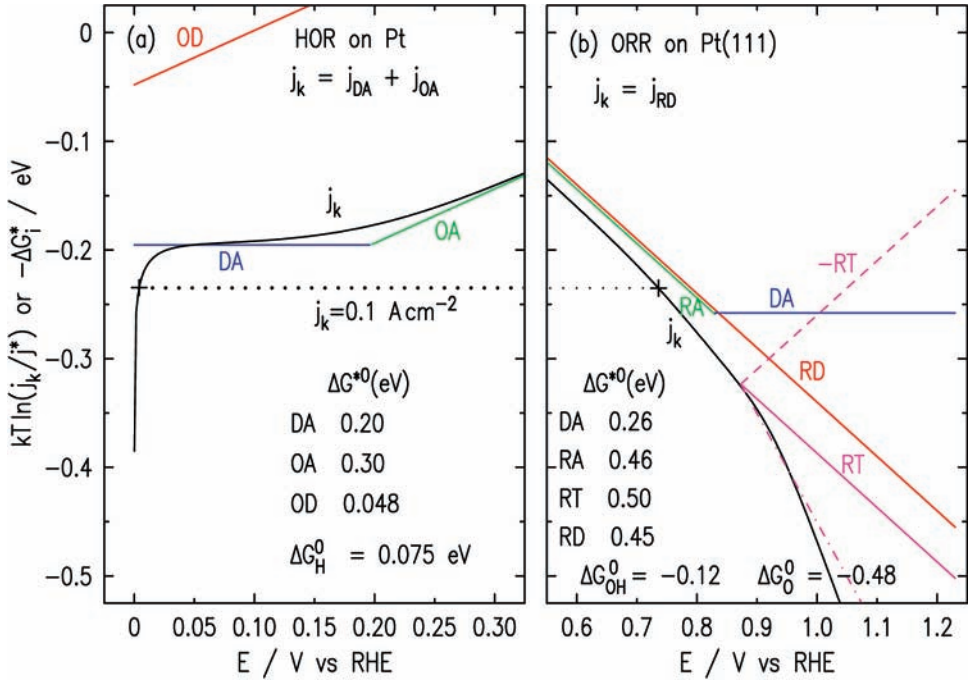

Figure 4. Activity-and-barriers plot for the HOR on polycrystalline Pt in H_2-saturated (1 atm) 0.1 M $HClO_4$ solution (a), and for the ORR on Pt(111) in O_2-saturated (1 atm) 0.1 M $HClO_4$ solution (b) at $T = 296$ K. Because the electron-transfer coefficients are 0.5 for all single electron-transfer reactions, the slope is 0.5 for oxidative reactions (OA, OD, and −RT), and −0.5 for reductive reactions (RA, RT, and RD), and DA remains potential-independent. The dotted-dashed purple line shows a slope of −1 at potentials positive of 0.873 V.

concentration is proportional to its partial pressure, P_{O_2}, we found from eqs 12 and 13,

$$\Delta(\Delta G^{*0}_{DA}) = \Delta(\Delta G^{*0}_{RA}) = -0.5kT\ln(10)\,\Delta(0.5\log c_{O_2}) = -0.03\log P_{O_2} \quad (47)$$

Similarly,

$$\Delta(\Delta G^{0}_{O}) = \Delta(\Delta G^{0}_{OH}) = -0.03\log P_{O_2} \quad (48)$$

In fitting θ_q, we also adjusted the reversible potential for the ORR using

$$E^0_{ORR} = 0.25kT\ln(10)\,\Delta(\log c_{O_2}) = 0.015\log P_{O_2} \quad (49)$$

Good fits were found with P_{O_2} smaller than 0.01 atm; the fit for 0.0005 atm is shown in Figure 2a, and Figure 2b plots the corresponding change in kinetic current. Lowering the oxygen concentration increases the barriers for adsorption, thereby downshifting the RA and DA lines. The kinetic current becomes largely adsorption-limited. At 0.8 V, the kinetic current at 0.0005 atm has fallen to 2% of the kinetic current at 1 atm oxygen pressure, a finding consistent with negligible ORR current in a deaerated solution.

Analyses using models other than the dual-path, symmetric β model, failed to produce explainable adsorption isotherms. For example, we tested the commonly proposed RA-only reaction models and the possibility of asymmetric electron-transfer coefficient, the latter affording a possible explanation for the low Tafel slope at high potentials. On the basis of theoretical calculations using a planar model and a nonplanar one, Anderson et al.[27] showed (in their Figure 8) the nearly linear potential dependence of the activation barrier between 1.2 and 0.7 V, with the slopes corresponding to $\beta = 0.92$ and 0.70, respectively. We found that the measured polarization curve can be fitted with β up to 0.6. The upper panels in Figure 3 reveal that reasonable fits can be obtained using a model with only the RA pathway (Figure 3a), or by fixing ΔG^{*0}_{DA} at 10 eV to effectively block the DA pathway in the dual-path model (Figure 3b), and by assuming $\beta = 0.6$ for all three reductive reactions (Figure 3c). However, their corresponding adsorption isotherms for the adsorbate comprising both O and OH all exhibit coverages lower than those measured in deaerated solution at all or some potentials, thereby violating the dependence of $\theta_O + \theta_{OH}$ on the oxygen concentration. Thus, we exclude the RA-only reaction models and the possibility for β being significantly different from 0.5.

5. Reaction Mechanisms

To better understand the results for the ORR, we compared it to the HOR using the activity-and-barrier plots in Figure 4. The parameters for the HOR on polycrystalline Pt given in Figure 4a were determined previously.[24] The OA and OD signify the oxidative adsorption and oxidative desorption of H, respectively, and the DA represents the dissociative adsorption of hydrogen. Because $\Delta G^{*0}_{OD} = 0.048$ eV is much smaller than those two for the adsorption reactions ($\Delta G^{*0}_{DA} = 0.196$ and $\Delta G^{*0}_{OA} = 0.294$ eV), the HOR on Pt is adsorption-limited. The closeness of the curve of the HOR kinetic current (black line) to the DA and OA lines demonstrates that the DA and OA are, respectively, the RDS at low and high potential regions. In contrast, the activity-and-barrier plot for the ORR on Pt(111) shows that the $kT\ln(j_k/j^*)$ curve is considerably lower than the DA and RA lines, especially at high potentials, suggesting that the ORR on Pt is desorption-limited.

The adsorption-limited HOR entails a low equilibrium H coverage at the active atop sites and a large exchange current. The fast, inversed exponential rise of the kinetic current at low potentials is determined by the quadratic exponential decrease of the backward reaction current as the H coverage falls exponentially. On the other hand, the desorption-limited ORR

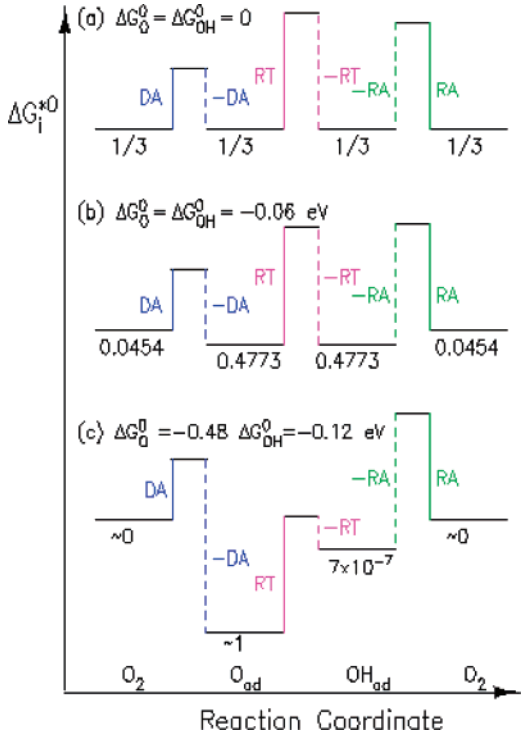

Figure 5. Free energy diagram for the DA, RT, and backward RA reactions at zero overpotential with the equilibrium coverage for each reaction stage. The lengths of the solid and dashed vertical lines represent the activation free energies of forward and backward reactions, respectively. The former remain the same, 0.26, 0.50, and 0.46 eV for the DA, RT, and RA reactions, respectively, and the latter varies with different adsorption free energies in the three cases.

exhibits a high O coverage at zero overpotential and a very small exchange current. At potentials positive of the O/OH reversible potential, the ORR activity drops with increasing potential about twice as fast as the variation of the barrier curve. This indicates a halving of the Tafel slope, which can be rationalized by the −RT line having the opposing effect on the kinetic current curve so that the slope of the $kT\ \ln(j_k/j^*)$ curve at $E \geq E_{O/OH}^{rev}$ is close to $d(-\Delta G_{RT}^*)/dE - d(-\Delta G_{-RT}^*)/dE = -0.5 - 0.5 = -1$ (dotted-dashed line in Figure 4b).

Electrocatalytic activities can be expressed as overpotentials for a given kinetic current. Figure 4 shows, using the plus signs, that the overpotential at 0.1 A cm^{-2} is 0.004 V for the HOR, and 1.23 − 0.736 = 0.494 V for the ORR. This half-volt difference in potential loss can be attributed mainly to the high activation barrier for the O to OH transition. For both reactions, dissociative adsorption is the dominant pathway at low overpotentials because it does not involve electron transfer and, thus, is potential-independent. Although the facile DA pathway is favorable for the HOR, it is detrimental for the ORR kinetics because of the deep energy trap for O.

6. Conclusions

We derived an intrinsic kinetic equation for the 4e-ORR in acidic media based on a model that comprises four essential elementary reactions forming two adsorption pathways and two reaction intermediates. To allow a wide range of rates for all four reactions, we did not assume a RDS. Instead, we used the activation free energies to describe the reaction barriers and derived the adsorption isotherms for O and OH by solving the steady-state rate equations. Analyzing the data for Pt(111) revealed that the DA and RA pathways coexist and the electron-transfer coefficient is 0.5 for the three reductive reactions. The activation free energies obtained from fitting experimental data are consistent with theoretical calculations.

Using the free energy diagram at zero overpotential and the activity-and-barrier plots, we illustrated that the 4e-ORR on Pt is desorption-limited because the dissociative adsorption is facile, and O and OH are strongly trapped on the surface. Above the reversible potential for the O and OH transition, the O coverage is high, causing severe inhibition of the ORR activity. As the O coverage falls with decreasing potential, the kinetic current increases with the lowering of the RD activation barrier and increasing the OH coverage. When OH coverage reaches a constant value at sufficiently low potentials, the Tafel slope is determined by the electron-transfer coefficient.

List of Symbols

c_{O_2}, c_{H^+}, M or mol cm^{-3} = concentrations of reactants

E, V = electrode potential versus reversible hydrogen electrode

E^0, V = reversible potential for the ORR

$E_{O/OH}^{rev}$, V = reversible potential for the adsorbed O ↔ OH transition

j, A cm^{-2} = measured current density

j_{DA}, j_{RA}, j_{RT}, j_{RD}, A cm^{-2} = partial kinetic current densities of elementary reactions

j_{DA}^0, j_{RA}^0, j_{RT}^0, j_{RD}^0, A cm^{-2} = intrinsic exchange current densities of elementary reactions

j_0, A cm^{-2} = exchange current density

j^*, A cm^{-2} = reference prefactor

j_k, A cm^{-2} = total net kinetic current density

j_f, A cm^{-2} = kinetic current for forward reactions

j_L, A cm^{-2} = mass-transport-limiting current density

k, eV K^{-1} = Boltzmann constant, 8.617×10^{-5}; $kT(296K)$ = 25.51 meV

k_i, k_{-i}, s^{-1} or $cm^3\ mol^{-1}\ s^{-1}$ = rate constants of elementary reactions, i = DA, RA, RT, RD

T, K = temperature

β = electron-transfer coefficient for reductive reactions

η, V = ORR overpotential

θ_q = coverage deduced from normalized integrated charge

θ_O, θ_{OH} = fractional coverage of reaction intermediates

θ_O^0, θ_{OH}^0 = equilibrium coverage, i.e., at $\eta = 0$

θ_O^∞, θ_{OH}^∞ = O and OH coverage at infinite overpotential

ν_i, mol s^{-1} cm^{-2} = reaction rates of elementary reactions, i = DA, RA, RT, RD

ΔG_O^0, eV = adsorption free energy for $^1/_2O_2 \rightarrow O_{ad}$ at $\eta = 0$

ΔG_{OH}^0, eV = adsorption free energy for $^1/_2O_2 + H^+ + e^- \rightarrow OH_{ad}$ at $\eta = 0$

ΔG_i^{*0}, eV = activation free energy at $\eta = 0$ for forward elementary reactions

ΔG_i^*, ΔG_{-i}^*, eV = potential dependent activation free energy

Appendix. Zero Net Reaction Rate for DA, RT, and RA Reactions at $\eta = 0$

On the basis of the rate equations at steady state (eqs 9 and 10), we found that the net RD reaction rate equals zero at $\eta = 0$, i.e., $\nu_{RD} = \nu_{+RD} - \nu_{-RD} = 0$, and that the net reaction rates for the DA, RT, and RA reactions obey the equation $\nu_{DA} = \nu_{RT} = -\nu_{RA}$. The latter equation seems to allow a nonzero net reaction rate for them at $\eta = 0$ because they form a reaction cycle, $O_2 \xrightarrow{DA} O \xrightarrow{RT} OH \xrightarrow{-RA} O_2$, that produces no net current or change of coverage. Here, we argue these net reaction rates

should be zero because there is no driving force to support a nonzero rate after equilibrium coverage is established.

Figure 5 shows the free energy diagrams for this reaction cycle with three different sets of adsorption free energies. Because ΔG_O^0 and ΔG_{OH}^0 are independent of reaction pathways, the equilibrium coverage for O and OH can be calculated using $\theta_O^0 = (e^{-\Delta G_O^0/kT})/(1 + e^{-\Delta G_O^0/kT} + e^{-\Delta G_O^0/kT})$ and $\theta_{OH}^0 = (e^{-\Delta G_O^0/kT})/(1 + e^{-\Delta G_O^0/kT} + e^{-\Delta G_O^0/kT})$. Then, the reaction rates can be compared using the products of $e^{-\Delta G_i^*/kT}$ and their corresponding coverage given in the figure.

The top panel shows the case when $\Delta G_O^0 = \Delta G_{OH}^0 = 0$, which has $\theta_O^0 = \theta_{OH}^0 = 1 - \theta_O^0 - \theta_{OH}^0 = 1/3$. Once equilibrium is established, activation free energy and coverage are equal in the forward and backward reaction directions for all three elementary reactions. Thus, the net reaction rates all are zero even though the absolute rates differ due to their different activation free energies. For example, suppose that the surface initially was free of adsorbate, then the coverage would increase faster for O than for OH because the activation barrier is smaller for DA than RA. The higher coverage for O than OH would make $\nu_{+RT} > \nu_{-RT}$. Once O and OH attain equilibrium coverage, the net rate for the RT reaction should fall to zero as the driving force vanishes. At the same time, adsorption ends as the net reaction rates for the DA and RT also fall to zero.

For $\Delta G_O^0 = \Delta G_{OH}^0 \neq 0$ (middle panel), $\theta_O^0 = \theta_{OH}^0$ is no longer equal to $1 - \theta_O^0 - \theta_{OH}^0$, but ν_{RT} still will fall to zero when the coverage for O and OH becomes equal.

Generally, when ΔG_O^0 differs from ΔG_{OH}^0 (bottom panel), ΔG_{RT}^{*0} and ΔG_{-RT}^{*0} also will be different. However, the net reaction rates still fall to zero when equilibrium is established because the difference in ΔG_{RT}^{*0} and ΔG_{-RT}^{*0} is compensated for by the difference between θ_O^0 and θ_{OH}^0.

Acknowledgment. This work is supported by the U.S. Department of Energy, Divisions of Chemical and Material Sciences, under Contract No. DE-AC02-98CH1-886.

References and Notes

(1) Damjanovic, A. Mechanistic Analysis of Oxygen Electrode Reactions. In *Modern Aspects of Electrochemistry*; Bockris, J. O. M., Conway, B. E., Eds.; Plenum Press: New York 1969; pp 369.

(2) Tarasevich, M. R.; Sadkowski, A.; Yeager, E. Oxygen Electrochemistry. In *Comprehensive Treatise of Electrochemistry*; Conway, B., Bockris, J. O. M., Yeager, E., Khan, S. U. M., White, R. E., Eds.; Plenum Press: New York 1983; Vol. 7, pp 301.

(3) Kinoshita, K. *Electrochemical Oxygen Technology*; John Wiley & Sons: New York, 1992.

(4) Appleby, A. J. *J. Electroanal. Chem.* **1993**, *357*, 117.

(5) Adzic, R. R. Recent advances in the kinetics of oxygen reduction. In *Electrocatalysis*; Lipkowski, J., Ross, P. N., Eds.; Wiley-VCH: New York, 1998; pp 197.

(6) Markovic, N. M.; Ross, P. N. Electrocatalysis at well-defined surfaces: Kinetics of oxygen reduction and hydrogen oxidation/evolution on Pt(hkl) electrodes. In *Interfacial Electrochemistry - Theory, Experiments and Applications*; Wieckowski, A., Ed.; Marcel Dekker: New York, 1999; pp 821.

(7) Ross, P. N., Jr. Oxygen reduction reaction on smooth single crystal electrodes. In *Handbook of Fuel Cells*; Vielstich, W., Lamm, A., Gasteiger, H. A., Eds.; Vol. 2, Electrocatalysis; Wiley: New York, 2003; Chapter 31, pp 465.

(8) Damjanovic, A. Progress in the studies of oxygen reduction during the last thirty years. In *Electrochemistry in Transition*; Murphy, O. J., Srinivasan, S., Conway, B. E., Eds.; Plenum Press: New York, 1992; pp 107.

(9) Bashyam, R.; Zelenay, P. *Nature* **2006**, *443*, 63.

(10) Stamenkovic, V. R.; Fowler, B.; Mun, B. S.; Wang, G. F.; Ross, P. N.; Lucas, C. A.; Markovic, N. M. *Science* **2007**, *315*, 493.

(11) Zhang, J.; Sasaki, K.; Sutter, E.; Adzic, R. R. *Science* **2007**, *315*, 220.

(12) Tian, N.; Zhou, Z. Y.; Sun, S. G.; Ding, Y.; Wang, Z. L. *Science* **2007**, *316*, 732.

(13) Adzic, R. R.; Zhang, J.; Sasaki, K.; Vukmirovic, M. B.; Shao, M.; Wang, J. X.; Nilekar, A. U.; Mavrikakis, M.; Uribe, F. *Top. Catal.*, in press.

(14) Shi, Z.; Zhang, J.; Liu, Z.; Wang, H.; Wilkinson, D. P. *Electrochim. Acta* **2006**, *51*, 1905.

(15) Nørskov, J. K.; Rossmeisl, J.; Logadottir, A.; Lindqvist, L.; Kitchin, J. R.; Bligaard, T.; Jonsson, H. *J. Phys. Chem. B* **2004**, *108*, 17886.

(16) Xu, Y.; Ruban, A. V.; Marvrikakis, M. *J. Am. Chem. Soc.* **2004**, *126*, 4717.

(17) Anderson, A. B.; Albu, T. V. *J. Electrochem. Soc.* **2000**, *147*, 4229.

(18) Wang, Y. X.; Balbuena, P. B. *J. Phys. Chem. B* **2004**, *108*, 4376.

(19) Stamenkovic, V.; Mun, B. S.; Mayrhofer, K. J. J.; Ross, P. N.; Markovic, N. M.; Rossmeisl, J.; Greeley, J.; Norskov, J. K. *Angew. Chem., Int. Ed.* **2006**, *45*, 2897.

(20) Gattrell, M.; MacDougall, B. Reaction mechanisms of the O_2 reduction/evolution reaction. In *Handbook of Fuel Cells*; Vielstich, W., Lamm, A., Gasteiger, H. A., Eds.; Vol. 2, Electrocatalysis; Wiley 2003; Chapter 30, pp 361.

(21) Markovic, N.; Gasteiger, H.; Grhur, B. N.; Ross, P. N. *J. Electroanal. Chem.* **1999**, *467*, 157.

(22) Wang, J. X.; Markovic, N. M.; Adzic, R. R. *J. Phys. Chem. B* **2004**, *108*, 4127.

(23) Wang, J. X.; Springer, T. E.; Adzic, R. R. *J. Electrochem. Soc.* **2006**, *153*, A1732.

(24) Wang, J. X.; Springer, T. E.; Liu, P.; Shao, M.; Adzic, R. R. *J. Phys. Chem. C* **2007**, *111*, 12425.

(25) Shao, M. H.; Liu, P.; Adzic, R. R. *J. Am. Chem. Soc.* **2006**, *128*, 7408.

(26) Hyman, M. P.; Medlin, J. W. *J. Phys. Chem.* **2006**, *110*, 15338.

(27) Anderson, A. B.; Cai, Y.; Reyimjan, A. S.; Kang, D. B. *J. Electroanal. Chem.* **2005**, *580*, 17.

(28) Wakabayashi, N.; Takeichi, M.; Itagaki, M.; Uchida, H.; Watanabe, M. *J. Electroanal. Chem.* **2004**, *574*, 339.